

Intrinsic fluorescence spectroscopy for endoscopic detection and localization of the endobronchial cancerous lesions

Yasser Fawzy

Perceptronix Medical, Incorporated
Suite 400, 555 W. 8th Avenue
Vancouver, BC V5Z 1C6
Canada

and
National Institute of Laser Enhanced Sciences (NILES)
Cairo University
Cairo, Egypt

Haishan Zeng

Cancer Imaging Department
BC Cancer Agency
675 W. 10th Avenue
Vancouver, BC V5Z 1L3
Canada

Abstract. Fluorescence spectroscopy contains diagnostic information about the lung biochemistry and morphology, including tissue optical properties and fluorophores. However, the fluorophore information is generally masked by the optical properties of the tissue, which complicates the evaluation of their role in lung-cancer detection. In this work, we have developed a method for extracting the intrinsic fluorescence spectra from the endoscopic measurements of the combined fluorescence and reflectance spectra. Principle components and classification analysis was performed to evaluate the diagnostic potential of the extracted intrinsic fluorescence spectra from *in vivo* combined fluorescence and reflectance spectral measurements. We evaluated the diagnostic sensitivity and specificity of both the intrinsic fluorescence and the fluorescence spectra. The results showed that the intrinsic fluorescence spectra contain significant diagnostic information that had been masked by the lung optical properties. We have also found that the intrinsic fluorescence has improved the specificity for endobronchial-cancer detection, although with a slight decrease in the detection sensitivity, when compared to the fluorescence spectra. This may indicate that intrinsic fluorescence analysis could be used to improve the diagnostic specificity of fluorescence spectroscopy and imaging. © 2008 Society of Photo-Optical Instrumentation Engineers. [DOI: 10.1117/1.3041704]

Keywords: fluorescence spectroscopy; tissue optics; reflectance spectroscopy; tissue fluorophores; lung cancer; cancer detection.

Paper 08029RR received Jan. 25, 2008; revised manuscript received Oct. 2, 2008; accepted for publication Oct. 6, 2008; published online Dec. 16, 2008.

1 Introduction

In recent years, fluorescence spectroscopy (FL) has emerged as an attractive technique for noninvasive, early diagnosis of cancer, including lung cancer, due to its sensitivity to subtle biochemical changes.¹⁻⁵ Such FL spectra contain rich biochemical information; however, it is difficult to extract this information from the measured spectra, because it gets strongly modulated by the wavelength-dependent absorption and scattering properties of tissue.^{6,7} The measured FL spectra contain hidden biochemical information of tissue fluorophores as well as tissue morphological information through the modulating wavelength-dependent scattering and absorption properties of tissue. Extraction of intrinsic fluorescence, by removing the distorting effects of scattering and absorption, allows one to separate the biochemical from the morphological information and therefore to develop optimal classification algorithms for tissue diagnosis. Considerable efforts have been made in the recent past to remove these distorting effects and to extract intrinsic FL spectra for various tissue-diagnosis applications.⁸⁻¹² However, as far as we know, the use of in-

trinsic FL spectra for lung-cancer detection and diagnosis has not been evaluated in previous studies. In this work, we developed, in the frame of the photon migration theory, a method for extracting the lung intrinsic FL spectra from the combined FL and reflectance spectra measured with our integrated white-light reflectance (WLR)/FL endoscopic imaging and spectroscopy system.¹³ Then we analyzed the extracted intrinsic FL spectra to investigate the potential of using intrinsic FL spectroscopy (IFL) for improving endobronchial-cancer detection in comparison to the (raw) FL. In the next section we present and discuss the materials and methods used for measuring and extracting the IFL spectra and the statistical methods used for analyzing the spectral data. Then we present and discuss the results and conclusions obtained from the IFL versus FL spectra.

2 Materials and Methods

2.1 Instrumentation

FL and reflectance spectra were measured during endoscopic examination using our integrated endoscopy system for simultaneous imaging and spectroscopy, described in detail in our

Address all correspondence to: Yasser Fawzy, Perceptronix Medical, Incorporated, Suite 400, 555 West 8th Avenue, Vancouver, BC, Canada V5Z 1C6. E-mail: yfawzy@cpinc.ca

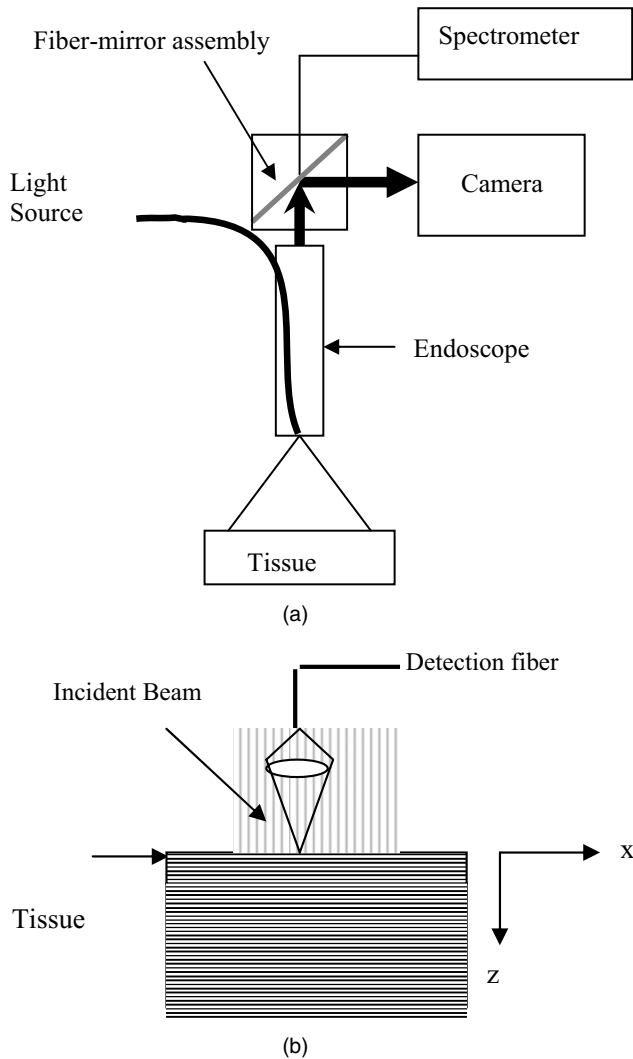


Fig. 1 (a) Schematic diagram of the combined imaging and spectroscopy endoscopy system used in the *in vivo* spectral measurements and (b) the equivalent geometry of our endoscopic noncontact spectral measurements.

previous work.¹³ The bronchial tissue was illuminated by the endoscope with a broad beam (~ 2 cm beam diam on tissue). The light source used was a Xenon arc lamp providing both white light (400–700 nm, 10 mW) for WLR imaging and reflectance spectral measurements and a strong blue light (400–460 nm, >50 mW) with weak near-infrared (NIR) light (720–800 nm, 4 mW) for FL imaging and FL spectral measurements. The illumination fiber bundle of the endoscope is interfaced to the light source to illuminate the bronchial tree, and the imaging bundle of the endoscope collects and relays the reflected and the FL signal from the tissue surface to the system for imaging and spectroscopy.

The spectral measurements were performed using a specially designed spectral attachment between the endoscope eyepiece and the camera (Fig. 1). As shown in Fig. 1, the light coming out of the endoscope is focused to form an interim image at a fiber-mirror assembly. This assembly is fabricated by drilling a hole through a mirror and mounting a 200- μm core-diameter taper fiber through the hole. The 200- μm opti-

cal fiber carries the optical reflectance signal or fluorescence signal from a spot at the center of the image, which corresponds to an area of 1 mm diameter at the tissue surface when the endoscope tip is 10 mm from the tissue surface, to the spectrometer (USB2000, Ocean Optics, Dunedin, FL) for spectral analysis. The system spectral resolution is 5 nm. We installed a movable bandpass (BP) filter (470–700 nm) at the spectrometer entrance to block the reflected blue and NIR light to facilitate fluorescence spectral measurements. As such, the fluorescence spectral-measurement wavelength ranges were restricted to between 470 and 700 nm, but the reflectance spectral-measurement range was between 400 and 700 nm. The spectrometer exposure time was set at 200 ms. The video image and the spectrum, in either the WLR or the FL mode, are displayed simultaneously on the computer monitor in live mode. A still image or a spectrum at any time point of interest during the endoscopy procedure can be captured and stored in the PC. The suspected lesions are identified using FL imaging and/or WLR imaging, and then both reflectance and FL spectra are acquired from the suspected (identified) lesions. The advantage of this system is that spectral measurements are performed in a noncontact manner through an intermediate image plane.¹⁴ Therefore, fiber probes are not needed to go through the instrument channel of the endoscope as often as in other literature, making clinical applications of this technology much more convenient. It also created a measurement geometry of broad-beam illumination and narrow-spot detection [Fig. 1(b)], simplifying theoretical modelling of the measured spectra.

2.2 IFL Model

The method used for extracting the IFL spectra was developed using the photon migration approach first proposed by Wu et al.⁸ In this method, it was assumed that the phase-function dependence of the scattering is separated from the scattering coefficient μ_s and the absorption coefficient μ_a by introducing an escape probability distribution function $f_n(g)$, which describes the probability of a photon with the scattering anisotropy coefficient g escaping from the tissue sample after n scattering events. Using this approach, and under the simplified assumption that $f_n(g)$ can be represented by an exponentially decreasing function of n , the diffuse reflectance R of a medium with uniform distribution of scatterers and absorbers can then be modeled as:¹⁰

$$R = \sum_{n=1}^{\infty} a^n f_n(g) = \frac{R_0 \epsilon a \exp(-\beta)}{1 - a \exp(-\beta)} \quad (1)$$

where $\epsilon = \exp(\beta) - 1$, $\beta = S(1-g)$, S is a constant that depends on the measurement geometry, R_0 is the reflectance in the absence of absorption, and the albedo $a = \mu_s / (\mu_a + \mu_s)$. Assuming the anisotropy g is independent of the wavelength within the investigated range, the intrinsic fluorescence spectra (line shape) for single excitation wavelength can be generated from:^{9,10}

$$f_{xm} = \frac{F_{xm}}{\frac{1}{\mu_{sx}} \left(\frac{R_{0x} R_{0m}}{\epsilon_x \epsilon_m} \right)^{1/2} \frac{R_x}{R_{0x}} \left(\frac{R_m}{R_{0m}} + \epsilon_m \right)} \quad (2)$$

where f , R , and F are the IFL, measured reflectance, and measured raw FL spectra, respectively. μ_s is the scattering coefficient, and x and m are indicators for the excitation and the emission wavelengths, respectively. Because the intensity information has not been used in our analysis, all the multiplicative factors that were included in the original expression by Feld et al.⁹ have been omitted from Eq. (2) above. This includes the quantity l that characterizes the given light delivery-collection and the quantity $\sqrt{\epsilon_x \epsilon_m}$.

For our setup, the excitation is done using an intense polychromatic light source producing wavelengths in the blue spectrum range between 400 and 460 nm. However, due to the decreasing transmission of the illumination light guide of the bronchoscope with decreasing wavelengths in the blue range, more than 70% of the transmitted light energy is within the 430–460 nm wavelength range, which limits the range of the effective excitation wavelengths within that specified band.

The resultant IFL can be obtained from:

$$IFL_{|x1}^{x2} = \int_{x1}^{x2} f_{xm}(x) d\lambda_x \quad (3)$$

where ($x1=430 \text{ nm} \rightarrow x2=460 \text{ nm}$) is the effective excitation wavelengths range. For simplification, we have assumed through our analysis that the line shape of the lung fluorescence emission is the same for all excitation wavelengths within the effective excitation range (430–460 nm). Although the fluorescence-emission intensity for many tissues depends on the excitation wavelength, our empirical observations and the previous lung fluorescence studies¹⁵ suggested that the line shape of the lung fluorescence emission does not change significantly for different excitation wavelengths and can be assumed constant for the excitation light range between 430 and 460 nm. However, our assumption is still an approximation, and for a broader excitation wavelength range, this assumption probably will not be accurate even for lung tissue.

From Eqs. (2) and (3) and with the modeling of the scattering coefficient using the power law $\mu_s \sim \lambda^b$, where b is the Mie scattering parameter,¹⁶ the intrinsic fluorescence line shape for our measurement geometry can be obtained as follows

$$IFL_{|x1}^{x2} = \left(\frac{\sqrt{R_{0m}} F_m}{R_m + R_{0m} [\exp(\beta) - 1]} \right) \sum \left(\frac{\sqrt{R_{0x}} \lambda_x^b}{R_x} \right) \quad (4)$$

For our analysis, the raw FL spectra (F_m), the emission-wavelength diffuse reflectance (R_m), and the excitation-wavelength diffuse reflectance (R_x) were obtained from the *in vivo* measurement. The Mie parameter for bronchial lesions showed slight changes from normal to cancer lesions^{17,18} and was assumed to be constant ($b=0.99$) in our analysis. This assumption was also motivated by the fact that the changes in the scattering coefficient (and consequently the Mie parameter) have a very weak effect on the line shape of the IFL

spectra.^{8,9} The other reflectance quantities (R_{0m} and R_{0x}) were derived from the measured reflectance spectra using the reflectance model developed in previous work by ourselves and others.^{18,19} Finally, the probe-specific parameter S was obtained from the fitting of Eq. (1) to Monte Carlo reflectance measurements simulating our diffuse reflectance geometry for known optical properties. The calculated value of S for our geometry was ~ 0.18 .

2.3 Clinical Measurements

The clinical measurements performed were part of an international clinical study consisting of five different clinical sites in Canada and Europe. In this study, patients with known or suspected malignancies of the lung and with a medical indication for a bronchoscopy were selected. The examination procedure used was white light and autofluorescence imaging as well as FL and reflectance spectral measurements of the bronchial tree using the instrument described in Section 2.1. For this study, FL and reflectance spectral pairs were measured from 60 different tissue sites on 40 patients. A biopsy sample was obtained for each measurement site to classify the measured tissue site into normal, benign, or malignant. The pathological diagnosis was coded according to the World Health Organization Lung Cancer classification.²⁰ The pathology examination of biopsies revealed that 40 measured tissue sites are normal/benign lesions (17 normal, 15 hyperplasia, and 8 mild dysplasia) and 20 are malignant lesions (3 severe dysplasia/carcinoma *in situ*, 2 small-cell lung cancers, 10 nonsmall-cell lung cancer, and 5 adenocarcinomas). Our analysis was to develop algorithms to classify the spectra into two groups: (i) malignant lesions for tissue pathology conditions that were moderate dysplasia or worse and (ii) normal tissue/benign lesions for tissue pathology conditions that were below moderate dysplasia. This binary classification is also consistent with clinical practice that group 1 lesions should be biopsied and treated (or monitored) while group 2 conditions could be left unattended. During routine clinical endoscopy examination, all suspected malignant lesions (group 1) should be biopsied while group 2 conditions are not biopsied. However, in this specially designed study, for each patient, an extra biopsy (and corresponding spectral measurement) was taken randomly from either a normal-looking area or a suspected benign lesion so that we could assess the performance of the spectral diagnosis relatively independent of the performance of the imaging diagnosis. All the IFL and FL spectra were saved in two groups (benign/normal and malignant) for data analysis.

2.4 Data Analysis

We have analyzed both the IFL spectra and the (measured raw) FL spectra to evaluate the diagnostic information that is useful for differentiating normal tissue/benign lesions from malignant lesions. To extract the actual line shape of the measured spectra and to reduce interpatient variation, each measured spectrum was normalized by its maximum intensity. Principle-component (PC) analysis was applied to all of the normalized IFL and FL spectra, and eigenvectors of the corresponding covariance matrix were then calculated. For classification-algorithm development, we have used the eigenvectors that account for 98% of the total variance. We found

that six PCs accounted for 98% of the total variance for both FL and IFL spectra. Classifiers based on these PC scores were generated to perform binary classification of the spectra into two diagnostic classes, malignant lesions (moderate dysplasia or worse) and benign lesions/normal tissue (mild dysplasia and below). To evaluate the quality of demarcating between malignant and benign/normal tissues, we have applied discriminant function analysis (DFA) to determine the discrimination function line that maximized the variance in the data between groups while minimizing the variance between members of the same group. The performance of the diagnostic algorithms rendered by the DFA models for correctly predicting the tissue status (i.e., benign/normal versus malignant) underlying each PC score set derived from the IFL or FL spectra was estimated using the leave-one-out, cross-validation method on the whole data set,^{21,22} in which we removed one case from the data set and the DFA-based algorithm was redeveloped and optimized using data of the remaining cases. The optimized algorithm was then used to classify the data set. This process was repeated until all the cases (data) were classified. The sensitivity and specificity were calculated from the results of the classification using the following expressions:

$$\text{Sensitivity} = \text{TP} / (\text{TP} + \text{FN})$$

$\text{Specificity} = \text{TN} / (\text{TN} + \text{FP})$ where TP is true positive, FN is false negative, TN is true negative, and FP is false positive. We used the Statistica software package (version 6, Stat-Soft Inc., Tulsa, OK) for the statistical analysis.

3 Results

In this section, we present the results obtained from the method used to extract the IFS spectra and from the statistical analyses of the extracted IFS line shape and the measured raw FL spectra.

Figure 2 shows the measured *in vivo* reflectance, *in vivo* FL, and extracted IFL spectra from a sample benign lesion and a sample malignant lesion. As shown in Fig. 2(a), as an example of benign lesion, the peak around 590 nm in the FL spectrum was removed for the extracted IFL spectrum, leaving only one peak located around ~510 nm. In Fig. 2(b), as an example of malignant lesion, the peak around 590 nm in the FL spectrum was also removed for the extracted IFL spectrum, leaving only one peak located around ~520 nm. Further investigation showed that the peak around 590 nm was not observed in a great majority of the extracted IFL spectra for both malignant and benign lesions. This confirms that the peak around 590 nm is a pseudo-fluorescence peak that is mainly related to the tissue-absorption properties (blood hemoglobin absorption) rather than the true fluorophore spectral profile, while the peak around ~510–520 nm is a signature of the intrinsic fluorophores of the endobronchial tree.

Figure 3(a) shows the mean raw FL spectra of all the benign lesions and the mean raw FL spectra of all the malignant lesions, while Fig. 3(b) shows the corresponding mean IFL spectra from the same lesions. It can be seen from the figure that the peak position of the mean FL line shape was around ~515 nm for the benign as well as the malignant group; in contrast, there was a change in the peak position of the mean IFL line shape between the benign group and the malignant group. We have quantified the shift in the peaks of FL and IFL

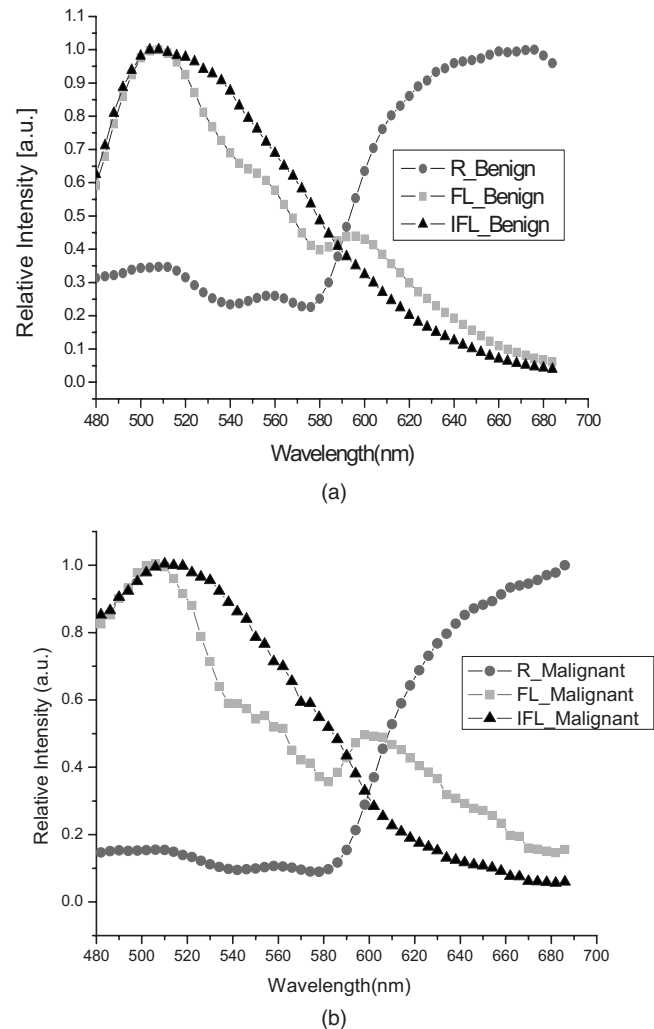


Fig. 2 Example measurements of (a) benign (hyperplasia) lesion and (b) malignant (nonsmall) lesion, showing the IFL spectra (triangles) extracted from the FL spectra (circles) and reflectance spectra (squares) measured from the same lesions.

spectra between benign and malignant groups by calculating the wavelength corresponding to the peak of the FL spectra and the IFL spectra for our data and applying the two-tailed t-test to evaluate the significance of this shift. The mean and the standard deviation of the peak wavelength for each group as calculated using the t-test is shown in Fig. 4. The results of the t-test show that there is shift in the peak wavelength of the IFL spectra between the benign group and the malignant group from ~515 to ~524 nm, respectively, with ($p=0.08$) compared to negligible shift ($p=0.65$) for that in the FL spectra.

Figure 5 shows the categorized scatter plot for the first and the second PCs for the FL and the IFL spectral data. It can be seen from the figure that the variations for both the FL spectra and the IFL spectra were larger for the malignant group compared to that in the benign group of the FL spectra and the IFL spectra, respectively. The line shapes of the first and second PCs were plotted against the wavelength (variables) in Fig. 6. The PC line shape was calculated from the whole spectral data (benign and malignant lumped together). As shown in

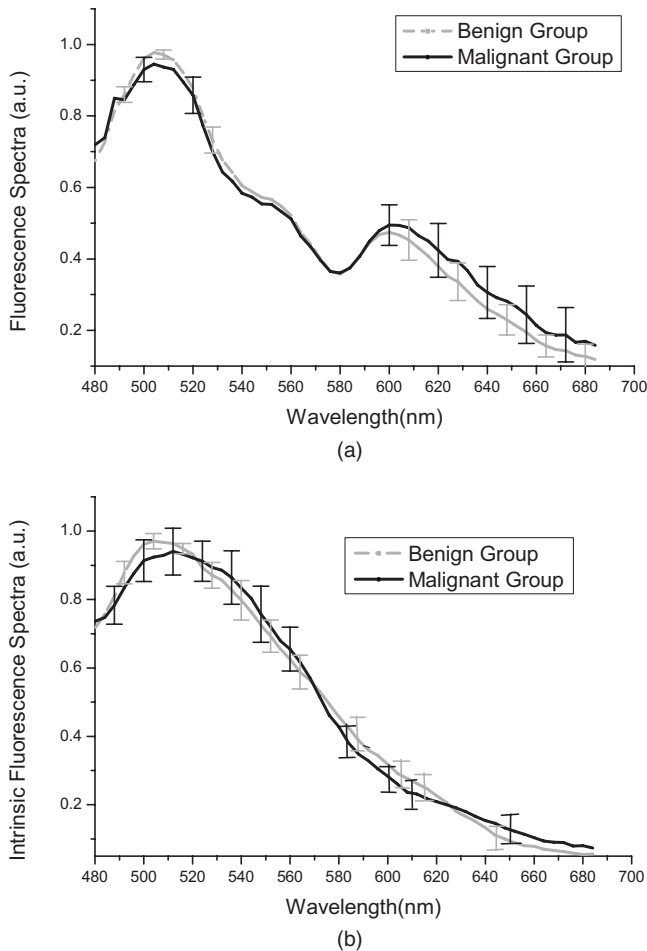


Fig. 3 The mean spectra of (a) the FL spectral measurements and (b) the IFL spectral data.

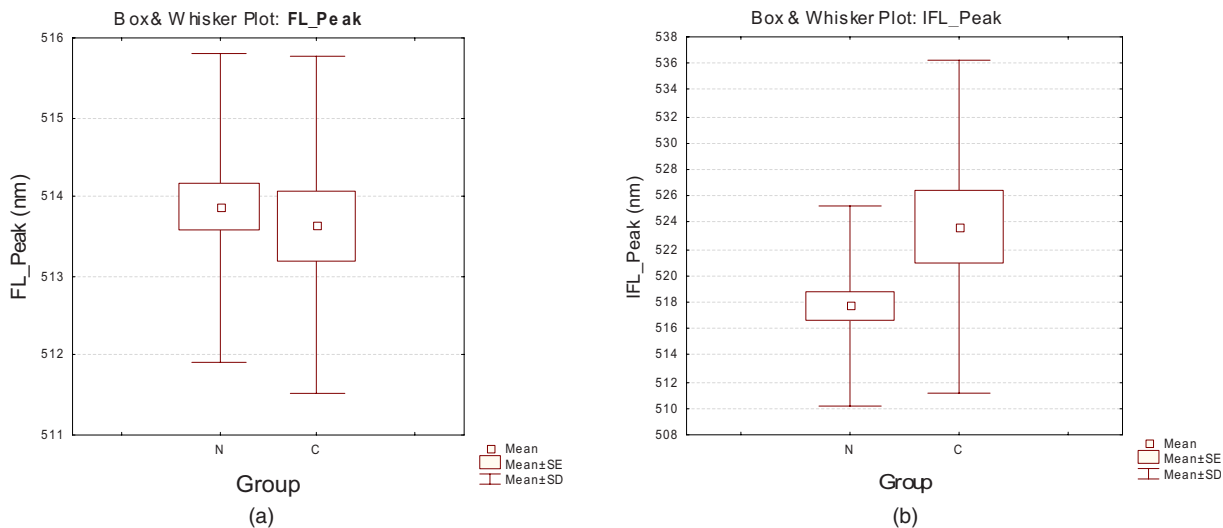


Fig. 4 The mean and the standard deviation of the peak wavelength for (a) FL spectra benign and malignant group and (b) IFL spectra benign and malignant group.

Fig. 6, the line shape of the first and second PCs of the FL spectra shows a signature peak around 580 nm that is likely related to oxy/de-oxyhemoglobin absorption. Such a signature peak was not found in the IFL spectra PCs. Figure 7 shows the binary plot for the first versus the second PC. As shown in the figure, the data from the malignant lesions are marked by wider variations for the FL as well as the FL spectra.

The diagnostic sensitivity and specificity of using IFL and FL spectra for differentiating malignant lesions from benign lesions/normal tissues are shown in Fig. 8. The sensitivity and specificity were estimated using the first two PCs for the FL spectra and the first three PCs for the IFL spectra. This was based on the results of the DFA, which showed that the F value (F to remove) for the variables used in the discriminate analysis was significant for the first two and three PCs for the FL and IFL spectra, respectively. We then calculated the diagnostic sensitivity and specificity for the FL and IFL spectra using the first two PCs of both spectra and the first three PCs of both spectra. The results of this analysis are reported in Fig. 8, which shows that, overall, the sensitivity of the FL spectra is higher than that of the IFL spectra. However, when the three PCs are used, the diagnostic specificity of the IFL spectra is relatively higher (70%) than that of the FL spectra (66%).

4 Discussion and Conclusions

Intrinsic fluorescence provides specific tissue biochemical information that could be valuable for measuring tissue fluorophores and for improving diagnostic accuracy for cancer detection. Many researchers have extracted and studied the intrinsic fluorescence that result from single-wavelength excitation of different tissues, such as the human aortic,⁸ the cervix,^{23,24} and the oral cavity.²⁵ In our study, we are extracting the intrinsic fluorescence of the endobronchial tree for polychromatic blue-light (400–460 nm) excitation and evaluating its potential for improving the diagnostic accuracy of lung-cancer detection and classification. Our results showed that IFL spectra, and consequently the endobronchial

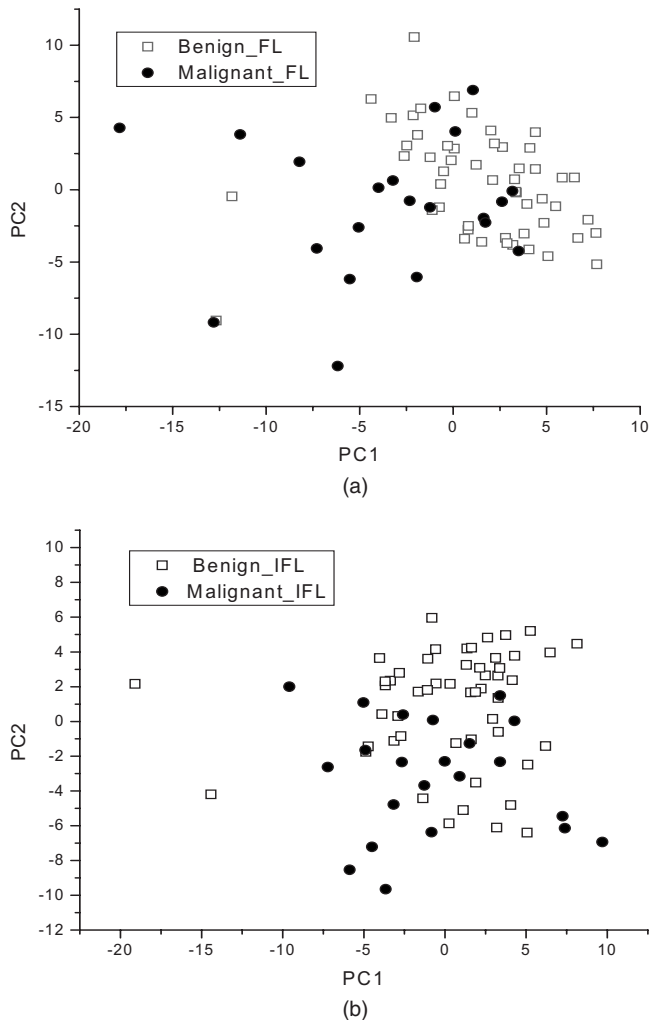


Fig. 7 Binary plot for the first PC versus the second PC for (a) the FL spectra and (b) the IFL spectra.

tree fluorophores, contain valuable diagnostic information for differentiating between benign and malignant lesions. Although detailed analysis of the tissue fluorophores has not been investigated in this study, our results suggest that the IFL

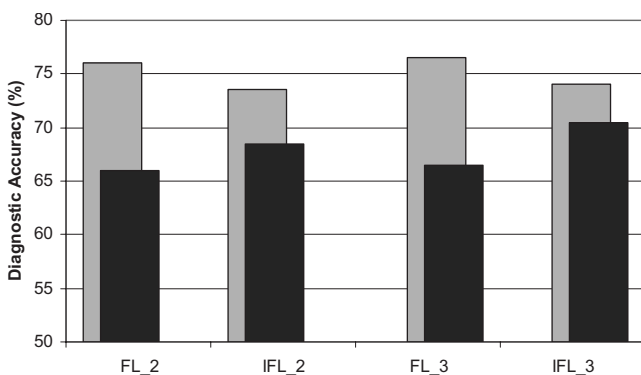


Fig. 8 Diagnostic sensitivity (dark gray) and specificity (light gray) when using two PCs for FL (FL_2) and IFL (IFL_2) analysis and when using three PCs (FL_3 and IFL_3).

peak is probably correlated to that of the structural protein (elastin and collagen) fluorescence.^{26,27} Our results indicate that there are indeed observed differences in the line shape of the IFL spectra between the benign and malignant lesions. In particular, a shift in the peak position between the benign group and the malignant group was observed in the IFL spectra, most likely due to the removal of the distorted effect caused by the optical properties, while the FL spectra showed negligible peak-position shift between the two groups. The results also showed that these observed differences in the IFL spectra could be useful for improving the cancer-detection specificity. However, the potential of using such differences for designing practical methods that improve diagnostic specificity without a loss in the diagnostic sensitivity needs further investigations.

Although many studies have investigated different methods for extracting the IFL spectra,^{8–12} fewer studies have investigated the potential of IFL spectra for improving the accuracy of cancer detection and classification. Georgakoudi et al.²⁸ assessed the potential of the IFL spectra, combined with diffuse reflectance and light-scattering spectroscopy, to improve the detection of cervical squamous intraepithelial lesions. They found, at 377 nm excitation wavelength, a change in both the intensity and the line shape of the IFL spectra between suspicious benign and malignant lesions. They also reported sensitivity and specificity of 62 and 67%, respectively, for classifying benign suspicious lesions versus malignant lesions. Kortum et al.^{29,30} investigated the potential of FL measurement and analysis for the *in vivo* detection of cervical intraepithelial dysplasia. They extracted the fluorophore concentration directly from the measured FL spectra using the model-based analysis approach. They found an increase in the flavin adenine dinucleotide fluorescence and a decrease in the stromal collagen fluorescence for dysplastic tissue compared to normal tissue.

The observed differences found in the IFL spectra between benign and malignant lesions indicate that the fluorophore concentration the biochemical environment, and the redox ratios may have been significantly altered during cancer progression. In addition, the relative specificity improvement using IFL spectra compared to that of the FL spectra may suggest that the changes in the biochemical environment, which are associated with both FL and IFL spectra, are more specific to the cancer compared to the changes in the epithelial thickness and tissue optical properties,³¹ which are associated with FL spectra but not IFL spectra. In particular, changes in epithelial thickness and optical properties could show similar trends for both benign and malignant lesions (e.g., benign lesions such as inflammation would have an increase in the absorption coefficient similar to that accruing in the malignant lesions), and these changes may mask the IFL spectral line-shape variations and are likely to be the major cause of the observed low specificity of the FL spectra diagnosis.

It should be emphasized that our device measures the spectra in a noncontact manner, but the endoscopic tip-tissue distance varies for different measurements. Our spectral measurement method is more practical from a clinical point of view, especially when compared to the contact probe measurement, which is inserted in the endoscope instrument channel. However, due to the noncontact nature of the measure-

ment, we are not retaining information about the intensity of the spectra and therefore only use the spectral line shape (the normalized spectra) for classifying benign lesions from malignant ones. Such intensity-related information measurement is expected to further improve the diagnosis of the FL spectra.^{32,33}

In summary, we have developed, in the frame of photon-migration theory, an analytical model that can be used to extract the IFL spectra from the measured raw *in vivo* FL spectra excited by polychromatic (400–460 nm) blue light using noncontact detection geometry. We have then analyzed the IFL spectra and evaluated the contained diagnostic information in comparison to the raw FL spectra. Future work will involve application of the method to more *in vivo* measurements and investigation of combining reflectance spectroscopy, FL, and IFL with WLR/FL imaging to improve diagnostic sensitivity and specificity for lung-cancer detection and localization.

References

1. S. Lam, J. Y. C. Hung, S. M. Kennedy, J. C. Leriche, S. Vedal, B. Nelems, C. E. MacAulay, and B. Paclic, "Detection of dysplasia and carcinoma in situ by ratio fluorometry," *Am. Rev. Respir. Dis.* **146**, 1458–1461 (1992).
2. S. Lam, T. Kennedy, M. Unger, Y. E. Miller, D. Gelmont, V. Rusch, B. Gipe, D. Howard, J. C. LeRiche, A. Coldman, and A. F. Gazdar, "Localization of bronchial intraepithelial neoplastic lesions by fluorescence bronchoscopy," *Chest* **113**, 696–702 (1998).
3. N. Ramanujam, M. Mitchell, A. Mahadevan, S. Thomsen, E. Silva, and R. Richards-Kortum, "Fluorescence spectroscopy: a diagnostic tool for cervical intraepithelial neoplasia (CIN)," *Gynecol. Oncol.* **52**, 31–38 (1994).
4. G. Wagnieres, W. Star, and B. Wilson, "In vivo fluorescence spectroscopy and imaging for oncological applications," *Photochem. Photobiol.* **68**, 603–632 (1998).
5. Y. Kusunoki, F. Imamura, and H. Uda, "Early detection of lung cancer with laser-induced fluorescence endoscopy and spectrofluorometry," *Chest* **118**, 1776–1782 (2000).
6. M. Keijzer, R. R. Kortum, S. L. Jacques, and M. S. Feld, "Fluorescence spectroscopy of turbid media: Autofluorescence of the human aorta," *Appl. Opt.* **28**, 4286–4292 (1989).
7. A. J. Durkin, S. Jaikumar, N. Ramanujam, and R. R. Kortum, "Relation between fluorescence spectra of dilute and turbid samples," *Appl. Opt.* **33**, 414–423 (1994).
8. J. Wu, M. S. Feld, and R. P. Rava, "Analytical model for extracting intrinsic fluorescence in turbid media," *Appl. Opt.* **32**, 3585–3595 (1993).
9. M. G. Muller, I. Georgakoudi, Q. Zhang, J. Wu, and M. Feld, "Intrinsic fluorescence spectroscopy in turbid media: disentangling effects of scattering and absorption," *Appl. Opt.* **40**, 4633–4646 (2000).
10. Q. Zhang, M. G. Muller, J. Wu, and M. S. Feld, "Turbidity-free fluorescence spectroscopy of biological tissue," *Opt. Lett.* **25**, 1451–1453 (2000).
11. N. C. Biswal, S. Gupta, and N. Ghosh, "Recovery of turbidity free fluorescence from measured fluorescence: an experimental approach," *Opt. Express* **11**, 3320–3331 (2003).
12. J. C. Finlay and T. H. Foster, "Recovery of hemoglobin oxygen saturation and intrinsic fluorescence with a forward-adjoint model," *Appl. Opt.* **44**, 1917–1933 (2005).
13. H. Zeng, M. Petek, M. T. Zorman, A. McWilliams, B. Paclic, and S. Lam, "Integrated endoscopy system for simultaneous imaging and spectroscopy for early lung cancer detection," *Opt. Lett.* **29**, 587–589 (2004).
14. M. Tercelj, H. Zeng, and B. Paclic, "Acquisition of fluorescence and reflectance spectra during routine bronchoscopy examinations using the ClearVu Elite device: Pilot study," *Lung Cancer* **50**, 35–42 (2005).
15. J. Hung, S. Lam, J. LeRiche, and B. Paclic, "Autofluorescence of normal and malignant bronchial tissue," *Lasers Surg. Med.* **11**, 99–105 (1991).
16. J. M. Schmitt and G. Kumar, "Optical scattering properties of soft tissue: a discrete particle model," *Appl. Opt.* **37**, 2788–2797 (1998).
17. Y. Fawzy, M. Petek, M. Zorman, and H. Zeng, "In-vivo assessment and evaluation of lung tissue morphologic and physiological changes from non-contact endoscopic reflectance spectroscopy for improving lung cancer detection," *J. Biomed. Opt.* **4**, 044003–12 (2006).
18. M. P. L. Bard, A. Amelink, V. N. Hegt, W. J. Graveland, H. J. C. M. Sterenborg, H. C. Hoogsteden, and J. G. J. V. Aerts, "Measurement of Hypoxia-related parameters in bronchial mucosa by use of optical spectroscopy," *Am. J. Respir. Crit. Care Med.* **171**, 1178–1184 (2005).
19. Y. Fawzy and H. Zeng, "Determination of scattering volume fraction and particle size-distribution in the superficial layer of a turbid medium using diffuse reflectance spectroscopy," *J. Appl. Opt.* **16**, 3902–3912 (2006).
20. E. Brambilla, W. D. Travis, T. V. Colby et al., "The new World Health Association Classification of lung cancer," *Eur. Respir. J.* **18**, 1059–1068 (2000).
21. R. W. Dillion and M. Goldstein, *Multivariate Analysis: Methods and Applications*, Wiley, New York (1984).
22. P. Lachenbruch and R. M. Mickey, "Estimation of error rates in discriminate analysis," *Technometrics* **10**, 1–11 (1968).
23. I. Georgakoudi, E. Sheets, M. Muller, V. Backman, C. Crum, K. Badizadegan, R. Dasari, and M. Feld, "Trimodal spectroscopy for the detection and characterization of cervical precancers in vivo," *Am. J. Obstet. Gynecol.* **186**, 374–382 (2002).
24. R. Drezek, K. Sokolov, U. Utzinger, I. Boiko, A. Malpica, M. Follen, and R. Richards-Kortum, "Understanding the contributions of NADH and collagen to cervical tissue fluorescence spectra: Modeling, measurements, and implications," *J. Biomed. Opt.* **6**(4), 385–396 (2001).
25. M. Muller, I. Georgakoudi, Q. Zhang, J. Wu, and M. Feld, "Intrinsic fluorescence spectroscopy in turbid media: disentangling effects of scattering and absorption," *Appl. Opt.* **40**, 4633–4646 (2001).
26. R. Gillies, G. Zonios, R. R. Anderson, and N. Kollias, "Fluorescence excitation spectroscopy provides information about human skin in vivo," *J. Invest. Dermatol.* **115** (suppl 4), 704–707 (2000).
27. H. Zeng and C. MacAulay, "Fluorescence spectroscopy and imaging for skin cancer detection and evaluation," in *Handbook of Biomedical Fluorescence*, M. A. Mycek and B. W. Pogue, Eds., pp. 315–360, Marcel Dekker, New York (2003).
28. I. Georgakoudi, E. Sheets, M. Muller, V. Backman, C. Crum, K. Badizadegan, R. Dasari, and M. Feld, "Trimodal spectroscopy for the detection and characterization of cervical precancers in vivo," *Am. J. Obstet. Gynecol.* **186**, 374–381 (2001).
29. S. Chang, Y. Mirabal, E. Atkinson, D. Cox, A. Malpica, M. Follen, and R. Kortum, "Combined reflectance and fluorescence spectroscopy for detection of cervical pre-cancer," *J. Biomed. Opt.* **10**(2), 024031 (2005).
30. S. Chang, N. Marin, M. Follen, and R. Kortum, "Model-based analysis of clinical fluorescence spectroscopy for in vivo detection of cervical intraepithelial dysplasia," *J. Biomed. Opt.* **11**(2), 024008 (2006).
31. J. Qu, C. MacAulay, S. Lam, and B. Paclic, "Laser-induced fluorescence spectroscopy at endoscopy: tissue optics, Monte Carlo modeling, and in vivo measurements," *Opt. Eng.* **34**, 3334–3343 (1995).
32. D. Goujon, M. Zellweger, A. Radu, P. Grojean, B. Weber, H. Bergh, P. Monnier, and G. Wagnieres, "In vivo autofluorescence imaging of early cancers in the human tracheobronchial tree with a spectrally optimized system," *J. Biomed. Opt.* **8**, 17–25 (2003).
33. M. Bard, A. Amelink, M. Skurichina, M. Bakker, S. Burgers, J. Meerbeck, R. Duin, J. Aerts, H. Hoogsteden, and H. Sterenborg, "Improving the specificity of fluorescence bronchoscopy for the analysis of neoplastic lesions of the bronchial tree by combination with optical spectroscopy: Preliminary communication," *Lung Cancer* **47**, 41–47 (2005).